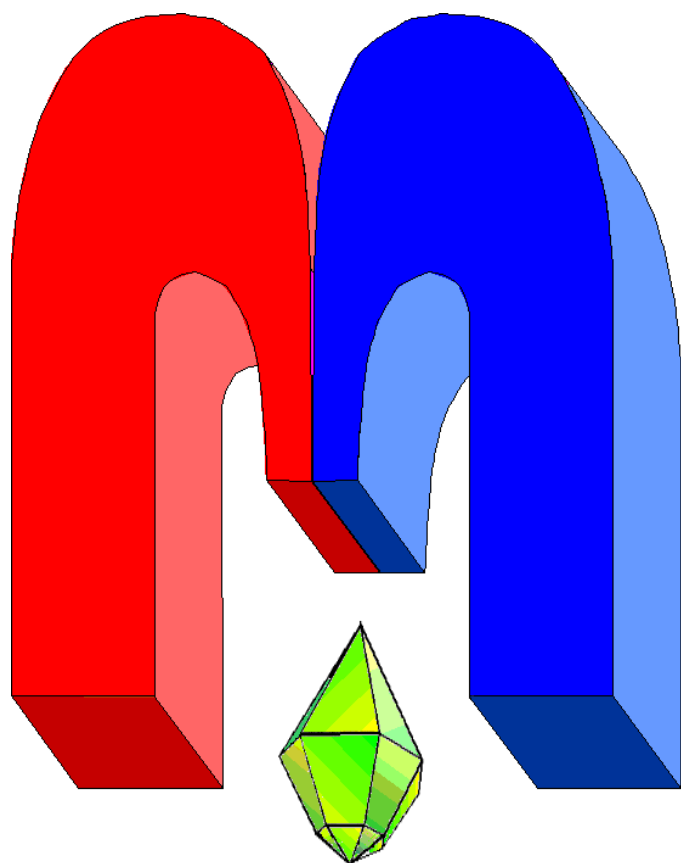


ISSN 2072-5981

doi: 10.26907/mrsej



***magnetic
Resonance
in Solids***

Electronic Journal

Volume 25

Issue 3

Article No 23303

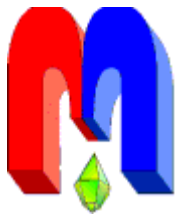
1-11 pages

2023

doi: [10.26907/mrsej-23303](https://doi.org/10.26907/mrsej-23303)

<http://mrsej.kpfu.ru>

<http://mrsej.ksu.ru>



Established and published by Kazan University*
Endorsed by International Society of Magnetic Resonance (ISMAR)
Registered by Russian Federation Committee on Press (#015140),
August 2, 1996
First Issue appeared on July 25, 1997

© Kazan Federal University (KFU)†

"Magnetic Resonance in Solids. Electronic Journal" (MRSej) is a peer-reviewed, all electronic journal, publishing articles which meet the highest standards of scientific quality in the field of basic research of a magnetic resonance in solids and related phenomena.

Indexed and abstracted by
Web of Science (ESCI, Clarivate Analytics, from 2015), Scopus (Elsevier, from 2012), RusIndexSC (eLibrary, from 2006), Google Scholar, DOAJ, ROAD, CyberLeninka (from 2006), SCImago Journal & Country Rank, etc.

Editor-in-Chief

Boris **Kochelaev** (KFU, Kazan)

Honorary Editors

Jean **Jeener** (Universite Libre de Bruxelles, Brussels)

Raymond **Orbach** (University of California, Riverside)

Executive Editor

Yurii **Proshin** (KFU, Kazan)
mrsej@kpfu.ru



This work is licensed under a [Creative Commons Attribution-ShareAlike 4.0 International License](https://creativecommons.org/licenses/by-sa/4.0/).



This is an open access journal which means that all content is freely available without charge to the user or his/her institution. This is in accordance with the [BOAI definition of open access](https://www.boai.ru/).

Technical Editor

Maxim **Avdeev** (KFU, Kazan)

Editors

Vadim **Atsarkin** (Institute of Radio Engineering and Electronics, Moscow)

Yurij **Bunkov** (CNRS, Grenoble)

Mikhail **Eremin** (KFU, Kazan)

David **Fushman** (University of Maryland, College Park)

Hugo **Keller** (University of Zürich, Zürich)

Yoshio **Kitaoka** (Osaka University, Osaka)

Boris **Malkin** (KFU, Kazan)

Alexander **Shengelaya** (Tbilisi State University, Tbilisi)

Jörg **Sichelschmidt** (Max Planck Institute for Chemical Physics of Solids, Dresden)

Haruhiko **Suzuki** (Kanazawa University, Kanazawa)

Murat **Tagirov** (KFU, Kazan)

Dmitrii **Tayurskii** (KFU, Kazan)

Valentine **Zhikharev** (KNRTU, Kazan)

* Address: "Magnetic Resonance in Solids. Electronic Journal", Kazan Federal University; Kremlevskaya str., 18; Kazan 420008, Russia

† In Kazan University the Electron Paramagnetic Resonance (EPR) was discovered by Zavoisky E.K. in 1944.

Analysis of the thermal treatment effects of gadolinium-containing hydroxyapatite by EPR method

A.Yu. Demina¹, N.V. Petrakova¹, F.F. Murzakhanov², G.V. Mamin², Yu.O. Nikitina¹, M.A. Sadovnikova^{2*}, S.O. Andreev³, A.V. Zhukov⁴, M.R. Gafurov², V.S. Komlev¹

¹A.A. Baikov Institute of Metallurgy and Materials Science, Russian Academy of Sciences, Moscow 119991, Russia

²Kazan Federal University, Kazan 420008, Russia

³St.Petersburg State University, Peterhof 198504, Russia

⁴D. Mendeleev University of Chemical Technology, Moscow 125480, Russia

*E-mail: margaritaasadov@gmail.com

(Received November 19, 2023; revised December 25, 2023;

accepted December 26, 2023; published December 29, 2023)

Hydroxyapatite (HAp)-based materials doped with rare earth elements (REE) have shown applications as biomaterials, lighting emitting materials, scintillating materials, in vivo imaging probes, and thermoluminescent dosimeters. Gadolinium-containing calcium phosphates are promising contrast agents for various bioimaging modalities. In this work, hydroxyapatite materials with gadolinium ion impurities with a 0.44 mol.% concentration were obtained by wet chemical precipitation. Samples after chemical synthesis (as-dried) and heat treatment were studied using electron paramagnetic resonance (EPR) spectroscopy in continuous wave and pulsed modes. Analysis of the EPR spectra made it possible to establish the incorporation of Gd³⁺ ions in the structure of HAp in two calcium positions with different parameters of the spin Hamiltonian. Heat treatment of samples at a $T = 1300^\circ\text{C}$ leads to a significant change in the EPR spectra of Gd³⁺ ions with a decrease of the uncontrolled nitrate anion centers (synthesis by-product) concentration.

PACS: 75.10.Dg, 76.30.-v, 75.20.

Keywords: rare earth elements, gadolinium, hydroxyapatite, electron paramagnetic resonance

1. Introduction

The development of calcium phosphate biomaterials to restore and heal injured bones is caused by the ongoing requirement to improve quality of life [1]. Despite significant progress in the design of implants based on titanium and tantalum alloys, zirconium dioxide or polymer compounds, calcium phosphate ceramics remains the most attractive bioactive inorganic materials. The main superiority and attractiveness of calcium-phosphate compounds, namely hydroxyapatite (HAp; molecular formula: $\text{Ca}_{10}(\text{PO}_4)_6(\text{OH})_2$), is due to the chemical and structural similarity with mineralized hard human tissue containing an intercellular matrix [2]. Considering a superior biocompatibility and osteoinductivity of calcium phosphates, their surface leads to stimulation of protein adsorption by biomaterial surfaces with favorable healing of the material interface and tissue leading to expanded bone formation [3]. Currently HAp is widely used as a bioceramic in different orthopedic and dental applications, bone tissue engineering, targeted drug and gene delivery [4].

The biological apatite (inorganic part of human hard tissue) differs considerably from synthetic HAp with a Ca/P ratio of 1.67 because of its stoichiometry, chemical/element composition, and crystallinity degree. The high crystalline synthetic HAp has slow bioresorption property resulting to a low capacity to form a connection with bone tissue or to promote new bone growth and worse interaction with the bone environment due to a slower rate of bone integration and adherence [5]. The solution of these challenges with a significant improvement

of physicochemical and biological properties can be carried out by ionic substitutions of the Ca^{2+} , PO_4^{3-} , or OH^- ions in the structure of the HAp. One of the structural features of HAp is the ability to accept a large diversity of ions (Na^+ , Li^+ , Mn^{2+} , Cu^{2+} , Al^{3+} , Fe^{2+} etc.) with different charge states in a wide range of concentrations (up to 20 mol.%), while the sample retains its initial spatial symmetry group $P6_3/m$ [6, 7]. These implemented ions have definite effect on the thermal stability, crystallinity degree, particle size, solubility, lattice parameters, morphology and bioactivity of HAp [8].

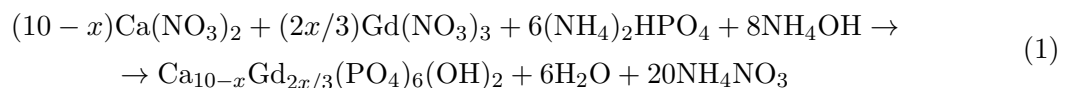
Recent studies have found that lanthanides, i.e., rare earth elements (REE) are also suitable for Ca^{2+} substitution in HAp [9]. The lanthanide ions have a well-known luminescent properties in the visible and near-infrared regions. The 4f-electronic configuration of REE originates the unique optical and magnetic features suitable for the preparation of magnetic resonance agents and highly sensitive diagnostic bioassays [10]. As an ideal host matrix for lanthanides, HAp satisfies many properties, including high resistance to luminescent centers, relatively low phonon energy, minimizing non-radiative relaxations, high chemical and thermal stability. The development of probes (contrast agents) for biomedical applications requires combination of materials with low toxicity levels with magnetic or fluorescence ability in order to be observed by confocal microscopy or magnetic resonance imaging (MRI) [11]. Among REE, gadolinium ions (Gd^{3+}) are the most studied and widely used contrast agent for MRI since the high-spin state ($S = 7/2$) and relaxation rate directly affect the brightness of the MRI scan and allows to create highly detailed images of cross-sections of internal organs [12]. Contrast agents containing Gd^{3+} are used to visualize tumors, infectious foci, the source of bleeding, metastases (secondary cancers), as well as areas of increased vascularization in breast tissue [13]. For tissue regeneration, each step of bone healing needs to be monitored carefully by imaging techniques, such as X-ray radiography, computed tomography (CT), single-photon emission computerized tomography (SPECT), and MRI. Interesting results were obtained for a related calcium-phosphate material, namely tricalcium phosphate (β -TCP) containing gadolinium ions with concentrations up to 0.1 mol.%. Metabolic and antibacterial activity studies have shown that the presence of Gd^{3+} ions in the β -TCP structure doesn't lead to an increase in the toxicity of the material while maintaining its biocompatibility [14].

One of the methods for calcium phosphate ceramics investigation is pulse electron paramagnetic resonance (EPR) [14], which allows distinguishing various paramagnetic impurities, determining their electronic relaxation times like spin-lattice (T_1) and spin-spin (T_2), the position of the impurity centers, etc. In the presented research we show some abilities of the pulsed EPR spectroscopy applied to the Gd-doped HAp.

2. Materials and methods

2.1. Synthesis

Chemical grade calcium nitrate tetrahydrate $\text{Ca}(\text{NO}_3)_2 \cdot 4\text{H}_2\text{O}$, gadolinium nitrate hexahydrate $\text{Gd}(\text{NO}_3)_3 \cdot 6\text{H}_2\text{O}$, diammonium phosphate $(\text{NH}_4)_2\text{HPO}_4$, and an aqueous solution of ammonia NH_4OH were used for precipitation of undoped HAp and Gd-doped HAp (Gd-HAp) in accordance with the following reaction:



where $x = ([\text{Ca}^{2+}] \cdot y)/100$; $y = 0$ and 0.25 mol. %.

The wet chemical precipitation was performed by dropwise adding of 300 ml of 0.5 M aqueous solution of $(\text{NH}_4)_2\text{HPO}_4$ to 500 ml of 0.5 M aqueous solution of $\text{Ca}(\text{NO}_3)_2$ to achieve the ratio of $\text{Ca}/\text{P} = 1.67$. The 6.25 ml of 0.1 M aqueous solution of $\text{Gd}(\text{NO}_3)_3$ was previously added to $\text{Ca}(\text{NO}_3)_2$ solution in the case of Gd-HAp synthesis to obtain the compound of general formula $\text{Ca}_{9.975}\text{Gd}_{0.017}(\text{PO}_4)_6(\text{OH})_2$. The low Gd concentration was chosen for the reasons of suitability for EPR detection of intentional dopants. The precipitation was carried out at constant stirring under room conditions. The pH level was maintained at 11.0 ± 0.5 by adding NH_4OH solution. The precipitate was exposed for aging during 7 days, then filtered with distilled water washing, and was dried at 70°C . The dried cake was ground to a fine powder and sieved through a mesh size of $100\ \mu\text{m}$. The as-dried HAp and Gd-HAp powders were also heat treated at 1300°C to reach well-crystallized HAp and to study the difference in structure features. The obtained powders were examined on phase composition and Gd content by the following methods: X-ray diffraction (XRD) analysis, Fourier transform infrared (FTIR) spectroscopy, determination of the specific surface area (SSA), X-ray fluorescence spectrometry (XFS).

2.2. Characterization

The XRD patterns were recorded using the D2 Phaser (Bruker, USA) diffractometer operating in Bragg-Brentano geometry with $\text{CuK}\alpha$ radiation ($\lambda = 1.5418\ \text{\AA}$), 2θ range from 10° to 70° , step size of 0.02° with 0.5 sec per step. Phases were identified using the JCPDS-PDF2 database [International Centre for Diffraction Data (ICDD)] [15]. The calculation of the lattice parameters (a , c), unit cell volume (V) and average crystallite size (D_{XRD}) was carried out using the Topas 5 software by the Rietveld method. The element content of gadolinium was determined using the XFS on the Spectroscan MAKC-GVM spectrometer (St. Petersburg, Russia).

EPR experiments were carried out using the functionality of the Bruker Eleksys E580 spectrometer with an operating microwave (MW) frequency of $\nu_{\text{MW}} = 9.6\ \text{GHz}$. Preliminary experiments were performed in continuous wave (CW) mode with constant MW irradiation ($P = 20\ \text{mW}$) at room temperature. The echo-detected EPR spectra was obtained by recording the integral intensity of the electron spin echo (ESE) at $T = 10\ \text{K}$ using $\pi/2 - \tau - \pi - \tau - \text{ESE}$ Hahn sequence with a change in the magnetic field \mathbf{B}_0 , where $\pi/2$ pulse duration is 16 ns. The spin-spin relaxation time T_2 was measured by tracking the primary amplitude of the ESE with the same pulse durations with a change of delay time τ . The spin-lattice relaxation time T_1 was extracted from inversion-recovery studies by applying the pulse sequence $\pi - T_{\text{delay}} - \pi/2 - \tau - \pi - \tau - \text{ESE}$, while the delay time T_{delay} varied. Simulation of the EPR spectra was carried out using the EasySpin program [16].

3. Results and discussion

The XRD patterns for heat treated HAp and Gd-HAp powders (Figure 1) consisted of the set of narrow high-intense peaks that was fully corresponded to HAp according to ICDD PDF card #[09-0432]. In order to assess the effect of Gd on the HAp structure, the lattice parameters (a and c) and unit cell volume (V) were calculated (Table 1). It was revealed the insignificant changes in HAp cell volume and small reducing in lattice parameters with Gd for Ca substitution. Although the number of refs mentioned slight increase in HAp lattice parameters with REE doping of low concentrations (up to $\text{REE}/(\text{Ca}+\text{REE}) = 0.05$) [17]. The Gd presence in Gd-HAp was confirmed by X-ray fluorescence spectrometry (XFS) performed on the heat treated powder. According to XFS results, the 1.41 wt.% Gd was contained in Gd-HAp that could be recalculated to 0.44 mol.% Gd for Ca in HAp. It could be concluded that the low Gd content

resulted in slight reducing of HAp lattice parameters and in decrease of average particle size (D_{XRD}) (Table 1). Also the very small amount of CaO was revealed by the presence of peak at $2\theta = 37.36^\circ$, which could be assigned to 100% peak for CaO of ICDD PDF card #[48-1467]. This pointed on slight deviation from HAp stoichiometry ($\text{Ca/P} > 1.67$) during synthesis. Detailing the XRD pattern of Gd-HAp, it was found a weak peak at $2\theta = 29.56^\circ$ which was absent in XRD pattern of undoped HAp and could be assigned to 100% peak of GdPO_4 phase ICDD PDF card #[83-0657]. It was reported that REE phosphate formation is accompanied to HAp formation, although at higher element concentration [18].

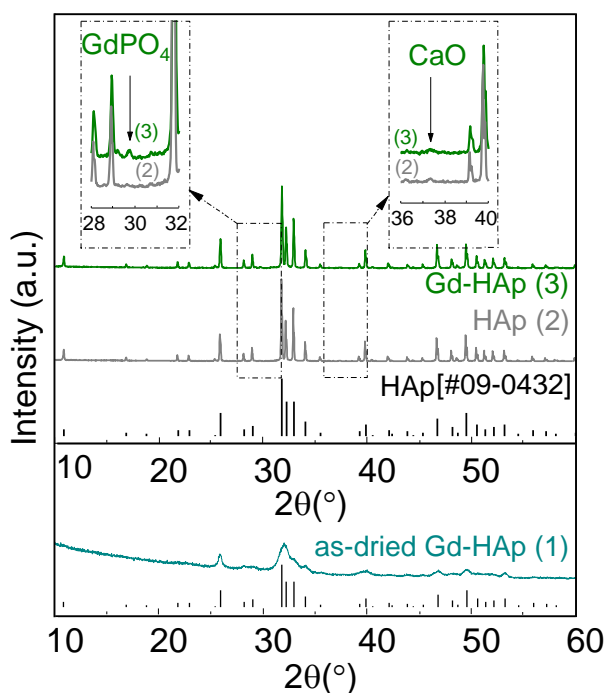


Figure 1. XRD for undoped HAp and Gd-HAp powders: (1) pattern for as-dried Gd-HAp quite consistent with the HAp (ICDD PDF card #[09-0432]), (2) pattern for heat treated undoped HAp according to ICDD PDF card #[09-0432]; (3) pattern for heat treated Gd-HAp also fully corresponds to HAp (ICDD PDF card #[09-0432]); the frame indicates the impurity of GdPO_4 according to ICDD PDF card #[83-0657] in heat treated Gd-HAp.

It was concluded, that precipitation by diammonium phosphate of calcium and gadolinium nitrates caused the formation of gadolinium orthophosphate hydrate along with HAp precipitation. It was highlighted that for REEs the orthophosphate hydrates of composition $((\text{REE})\text{PO}_4) \cdot [0.5 \leq \text{H}_2\text{O} \leq 3]$ of hexagonal structure form in an aqueous system containing ammonium phosphates. It was not possible to identify the presence of the intended compound in the obtained amorphous precipitates with low Gd content. It is known that the phosphates of light REE under heat treatment above 500°C transform to monoclinic phase and then above 1700°C – to tetragonal phase. Thus, the monoclinic GdPO_4 was detected in the sample of Gd-HAp heat treated at 1300°C . As density for GdPO_4 (6.001 g cm^{-3}) is rather higher than for HAp (3.08 g cm^{-3}), it was determined quite well even in small concentrations.

The HAp is initially paramagnetically pure and doesn't contain particles with an electron magnetic moment in the structure (EPR silent). Figure 2 shows the CW EPR spectra of HAp containing impurity gadolinium ions with a concentration of 0.44 mol.%. The rare-earth gadolinium ion Gd^{3+} with a $4f^7$ configuration in the main $^8\text{S}_{7/2}$ state is paramagnetic, and has an

Table 1. Results of the Rietveld refinement of XRD patterns for heat treated HAp and Gd-HAp powders: a and c are unit cell parameters; V is unit cell volume; D_{XRD} is average crystallinity size.

Sample	a , Å	c , Å	V , Å ³	D_{XRD} , nm
HAp	9.4231(8)	6.8844(8)	529.41(8)	380(7)
Gd-HAp	9.4216(8)	6.8836(6)	529.16(7)	230(6)

electron spin $S = 7/2$ with a zero orbital moment $L = 0$ [19]. The spectrum of this spin system should contain $2S = 7$ different magnetic transitions, which give 7 lines in the EPR spectrum with the center of gravity of the spectrum at $g \approx 2.0$, because there is no orbital magnetic moment. Figure 2(a) shows the EPR spectrum for a HAp as-dried, which was not subjected to heat treatment. HAp crystallizes in the hexagonal space group $P6_3/m$ and the gradient of the internal crystalline (electric) field leads to the appearance of a “zero field splitting” (ZFS) of the spin sublevels. As a result, we observe fine structure lines in the EPR spectrum. The Gd-HAp sample under study is in the form of a powder, therefore, all equally probable orientations of nanocrystals relative to the external magnetic field \mathbf{B}_0 are present in the EPR spectrum. The energy values of the ZFS depends on the relative position of the main crystallographic c -axis of the nanocrystal with the external magnetic field \mathbf{B}_0 direction. Thus, the components of the fine structure have an angular dependence, which causes mutual overlap and broadening of the available resonant absorptions [20]. The formation of low-field singularities, despite the powder phase of the sample and the high spin $S = 7/2$ of the impurity center, arises due to the unusual behavior orientation dependence of the spin levels [21]. The presence of the characteristic low-field EPR signals with effective g -factors ($g_{\text{eff}} = 5.59$, $g_{\text{eff}} = 2.84$ and $g_{\text{eff}} = 1.98$) [22–24] and corresponding theoretical simulation (Figure 2(a), blue line) allow to make unambiguous conclusions that the gadolinium ion has a valence of $3+$, and it is embedded in the HAp crystal lattice into one of the calcium positions Ca^{2+} . In this work, the authors do not discuss the mechanism of charge compensation, since this problem requires additional experimental affords and calculations by the density functional theory (DFT) method [25].

To describe the obtained powder form EPR spectra with Gd^{3+} ions we used the following spin Hamiltonian from the crystal field theory [26]:

$$H = g\mu_B\mathbf{B}_0\mathbf{S} + B_2^0O_2^0 + B_2^2O_2^2 + B_4^0O_4^0 + B_6^0O_6^0, \quad (2)$$

where g is g -factor, μ_B is the Bohr magneton, \mathbf{B}_0 is magnetic field induction vector, \mathbf{S} is the electron spin operator, B_q^k are the crystal field parameters, O_q^k are the Stevenson operators. Crystal field parameters for describing EPR spectra obtained in CW mode are listed in Table 2.

Heat treatment ($T = 1300^\circ\text{C}$) significantly changes the behavior of the absorption spectrum as

Table 2. Zero field splitting parameters Gd-HAp.

	B_2^0	B_2^2	B_4^0	B_6^0
Ca(1)	3580 MHz	-	390 MHz	300 MHz
Ca(2)	1500 MHz	120 MHz	-	-

shown in Figure 2(b). The resonant absorption lines look quite structured with the possibility of separating 7 groups of resolved lines in accordance with the electron spin of the Gd^{3+} ion. The linewidth of the central transition at g -factor 2.00 is only $B_{\text{PP}} = 0.1$ mT, which indicates that the Gd^{3+} isn't in the crystal structure of the HAp, but in a side phase with cubic symmetry. The most likely reason is associated with the formation of a CaO crystal [27] with gadolinium

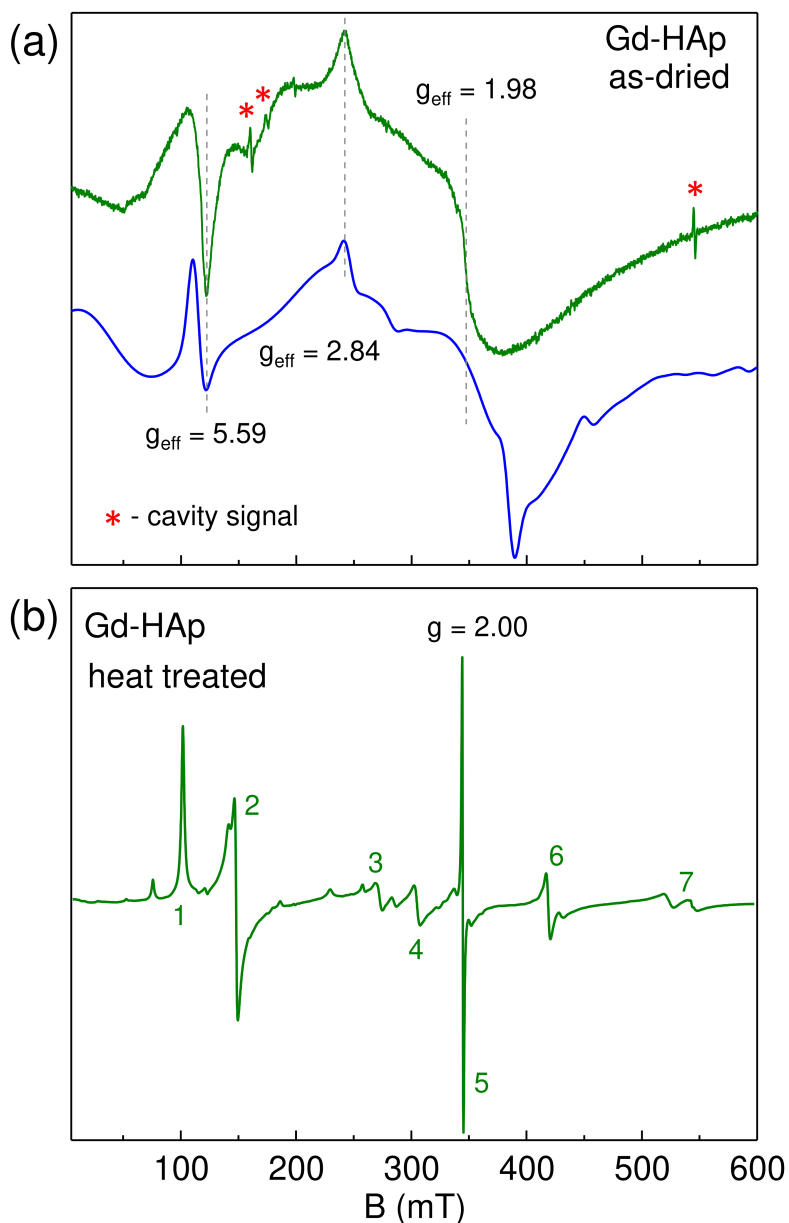


Figure 2. CW EPR spectra for Gd-HAp, where (a) the as-dried sample, green line is experiment, blue line is simulation. Narrow lines (170 mT, 200 mT, 550 mT) are cavity signals and don't belong to the sample under study; and (b) the sample after heat treatment at 1300°C. Observed narrow isotropic lines correspond to spin transitions of Gd^{3+} with $S = 7/2$ in CaO phase according to the selection rule $\Delta M_s = \pm 1$, namely (1, 7) $\pm 7/2 \leftrightarrow \pm 5/2$, (2, 6) $\pm 5/2 \leftrightarrow \pm 3/2$, (3, 5) $\pm 3/2 \leftrightarrow \pm 1/2$ and (4) $+1/2 \leftrightarrow -1/2$.

ions, which occurs when HAp decomposes. In the case of a CaO crystal, the Gd^{3+} ion is no longer affected by the electric field gradient, and thus narrow EPR lines are observed.

It is well known that rare earth ions, including gadolinium, due to the 4f electron configuration and spin-orbit coupling, have short relaxation times [28]. Consequently, all further echo-detected EPR experiments were carried out at low temperatures ($T = 10$ K). ESE EPR spectra are shown in Figure 3.

During the recording of the spectrum, MW pulses were used to precisely rotate the longi-

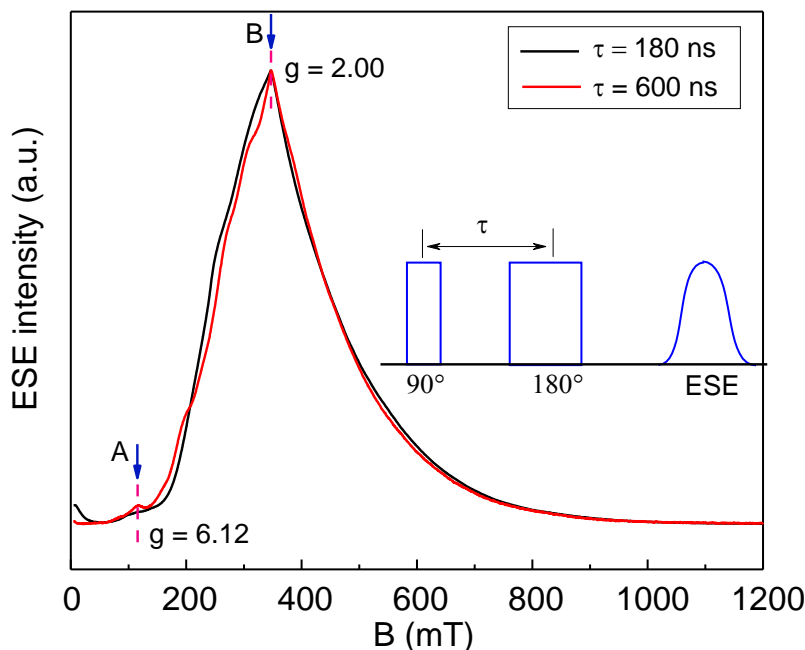


Figure 3. ESE EPR spectra for Gd-HAp the as-dried sample recorded for two different τ values in the pulse sequence.

tudinal magnetization M_z by 90° and then by 180° . The EPR spectrum was obtained for two different values of the delay between pulses in the sequence in order to establish short-lived paramagnetic centers. It is assumed that in the presence of different contributions with different values of relaxation times T_2 , intensity redistribution is expected, as was previously established in the work [26].

A comparative analysis in Figure 3 shows that the intensity and lineshape of the EPR spectrum is practically independent of the time delay. The result obtained assumes a uniform (homogeneous) distribution of Gd^{3+} ions within the HAp without the formation of synthesis side phases (oxide, by-products, etc.). An insignificant change in the intensity of resonant absorption in the low-field region is caused by the probability of spin transitions. The intensity of each of these lines will be proportional to the square of the matrix element $S_x = \sqrt{S(S+1) - M_s(1)M_s(2)}$ i.e., maximum for the transition $M_s = -1/2 \leftrightarrow 1/2$ and minimum for $M_s = -7/2 \leftrightarrow 5/2$. The $M_s(1,2)$ correspond to two projections of the Gd^{3+} electron magnetic moment, between which a resonance spin transition occurs with $\Delta M_s = \pm 1$. The gadolinium ion in the role of a contrast agent acts as a “catalyst” for the relaxation processes of hydrogen nuclei in the biological environment [29]. The lower limit of possibilities of shorting (reduction) of nuclear spin-lattice relaxation T_{1N} is determined by the electronic subsystem of Gd^{3+} ions. Thus, a quantitative estimate of the spin-spin and spin-lattice relaxation times of gadolinium ions has been established, which is presented in Table 3. The Gd^{3+} ion relaxation times were measured for two different magnetic fields (which differ by about 3 times) at points A and B in Figure 3, because these magnetic fields correspond to contributions from different paramagnetic centers in β – TCP [14]. Since the relaxation times are approximately in the same order of magnitude within the confidence interval, this most likely indicates that the Gd^{3+} ion occupies one of the two Ca^{2+} positions.

The using of nitrate salts as initial reagents during the chemical synthesis (1) of HAp leads

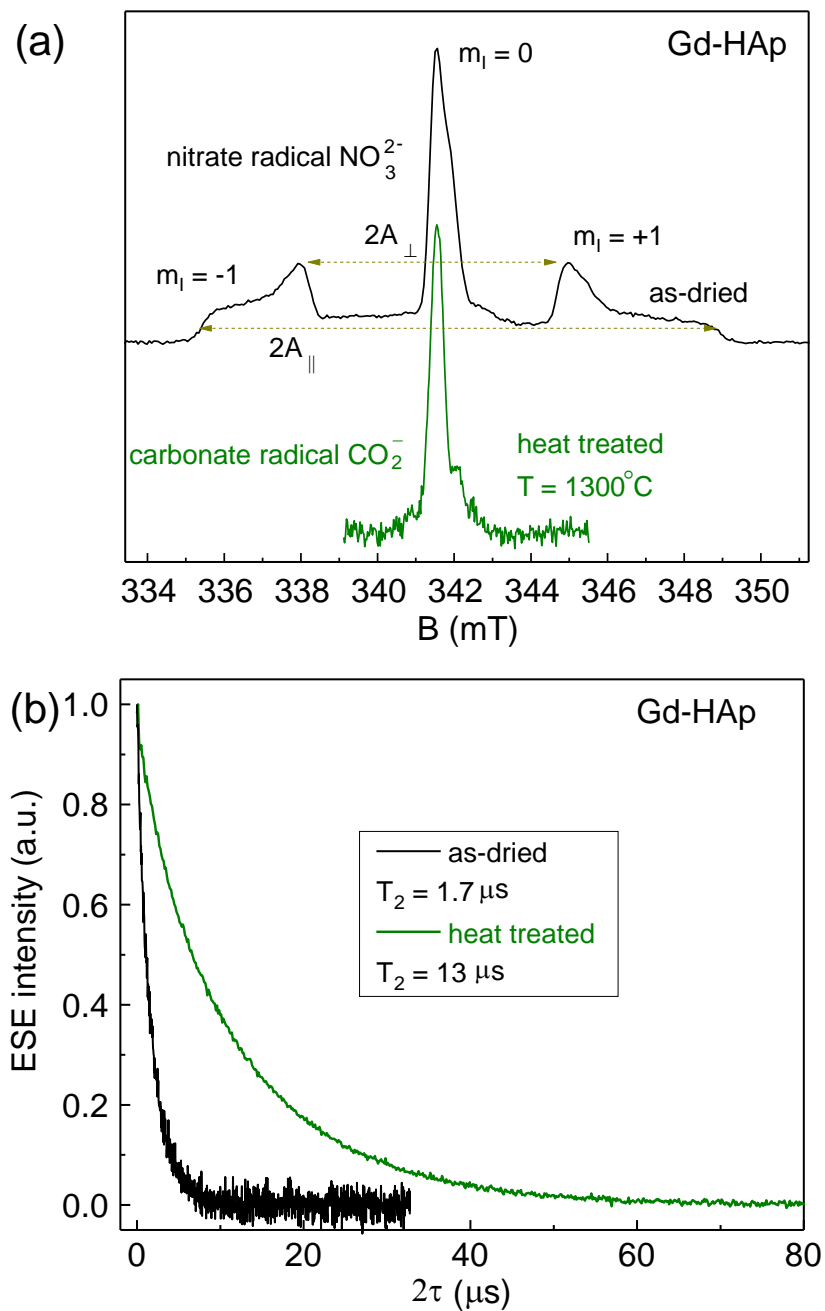


Figure 4. (a) ESE EPR spectra of radiation-induced centers in a HAp with gadolinium ions impurities; (b) Relaxation time curves of defect centers for as-dries samples (dark line) and heat treated (green line).

to the incorporation of NO_3^- complexes [30]. Anion centers act as an electron trap, and in the case of “capture” of a free electron, the nitrate complex transitions to a paramagnetic state with electron spin $S = 1/2$. The nitrogen radical localized in the crystal lattice structure can serve as a spin probe to obtain additional spectroscopic information [31]. The prepared samples as-dried and after heat treatment were irradiated with an X-ray source to create stable NO_3^{2-} paramagnetic centers [30]. Figure 4(a) shows the EPR spectra of radiation-induced centers for as-dried and after heat treatment materials. The interaction of the electron spin ($S = 1/2$) and the nuclear magnetic moment ($I = 1$, ^{14}N) leads to the formation of three hyperfine components (m_I) with splitting values $A_{\perp} = 70$ G and $A_{\parallel} = 133$ G corresponding to the single phase of

Table 3. Relaxation times of Gd^{3+} ions in Gd-HAp.

B_0, mT	$T_1, \mu\text{s}$	$T_2, \mu\text{s}$
347	81.8	1.2
117	54.6	0.9

HAp [32]. Heat treatment of the sample leads to the complete disappearance of synthesis by-products and a corresponding reduction of defects in the crystal lattice, as shown in Figure 4(a). The EPR spectrum of hydroxyapatite after heat treatment (bottom, green line in Figure 4(a)) contains a small amount of a carbonate radical with a low concentration within the sensitivity of the spectrometer. This procedure helps to reduce the amount of toxic nitrate radicals and increase the degree of crystallinity. Figure 4(b) also shows changes in the dynamic characteristics of radiation-induced centers at room temperature. Previously, relaxation times for nitrogen and carbonate radicals were established for pure hydroxyapatite samples, namely $T_2 = 11 \mu\text{s}$ for heat treatment and $T_2 = 3 \mu\text{s}$ for as-dried [32] measured at room temperature. The transverse relaxation time strongly depends on the radiation dose, so the authors suggest that the main mechanism for T_2 is spin-spin interaction. A comparative analysis of the curves shows that a change in the number of defects leads to a decrease in the spin-spin interaction between paramagnetic centers and, as a consequence, to an increase in the transverse relaxation time (T_2) by 7.6 times. Gadolinium ions don't have a significant effect on the relaxation characteristics of the nitrogen radical through dipole-dipole interaction, as was the case with impurity centers of Mn^{2+} [33] and Al^{3+} [25].

4. Conclusion

In this work, powders of synthetic hydroxyapatite ceramics doped by gadolinium ions with a concentration of 1.41 wt.% (0.44 mol.%) were obtained by wet chemical precipitation. Samples after chemical synthesis (as-dried) and heat treatment were studied using EPR spectroscopy in CW and pulsed modes. Analysis of the EPR spectra made it possible to establish the presence of Gd^{3+} ions in the structure of HAp in two calcium positions with different parameters of the spin Hamiltonian. Temperature treating of samples at a 1300°C leads to a significant change in the EPR spectra of Gd^{3+} ions with a decrease of the impurity anion centers (nitrate radical) concentration.

The study of the effect of the introduction of gadolinium ions into HAp on the electronic relaxation characteristics of stable nitrate radicals, including after heat treatment in air at 1300°C , suggests that nitrate anions and Gd^{3+} cations are located in the HAp structure within the same unit cell. It can be assumed that the co-doping of these ions in the proposed synthesis method is energetically more favorable than the separate introduction of ions, as we have shown earlier in the case of co-doping of HAp with nitrate anions and manganese (II) ions [34]. Detailed experimental and computational studies of the effects of doping and co-doping, and the establishment of charge compensation mechanisms are the subjects of our future studies.

Acknowledgments

Authors acknowledge the Russian Science Foundation Grant No. 23-63-10056 for financial support of this study.

References

1. Hou X., Zhang L., Zhou Z., Luo X., Wang T., Zhao X., Lu B., Chen F., Zheng L., *Journal of Functional Biomaterials* **13**, 187 (2022).
2. Zhou H., Lee J., *Acta Biomaterialia* **7**, 2769 (2011).
3. Prakasam M., Locs J., Salma-Ancane K., Loca D., Largeteau A., Berzina-Cimdina L., *Journal of Functional Biomaterials* **6**, 1099 (2015).
4. Vahabzadeh S., Roy M., Bandyopadhyay A., Bose S., *Acta Biomaterialia* **17**, 47 (2015).
5. Dorozhkin S. V., *Biomaterials Science* **9**, 7748 (2021).
6. Jiang Y., Yuan Z., Huang J., *Materials Technology* **35**, 785 (2020).
7. Ressler A., Žužić A., Ivanišević I., Kamboj N., Ivanković H., *Open Ceramics* **6**, 100122 (2021).
8. Arcos D., Vallet-Regí M., *Journal of Materials Chemistry B* **8**, 1781 (2020).
9. Ignjatović N. L., Mančić L., Vuković M., Stojanović Z., Nikolić M. G., Škapin S., Jovanović S., Veselinović L., Uskoković V., Lazić S., Marković S., Lazarević M. M., Uskoković D. P., *Scientific Reports* **9**, 16305 (2019).
10. Neacsu I. A., Stoica A. E., Vasile B. S., Andronescu E., *Nanomaterials* **9**, 239 (2019).
11. Gu M., Li W., Jiang L., Li X., *Acta Biomaterialia* **148**, 22 (2022).
12. Wahsner J., Gale E. M., Rodríguez-Rodríguez A., Caravan P., *Chemical Reviews* **119**, 957 (2018).
13. Liu Y., Tang Y., Tian Y., Wu J., Sun J., Teng Z., Wang S., Lu G., *ACS Applied Nano Materials* **2**, 1194 (2019).
14. Fadeeva I. V., Deyneko D. V., Barbaro K., Davydova G. A., Sadovnikova M. A., Murzakhhanov F. F., Fomin A. S., Yankova V. G., Antoniac I. V., Barinov S. M., Lazoryak B. I., Rau J. V., *Nanomaterials* **12**, 852 (2022).
15. Gates-Rector S., Blanton T., *Powder Diffraction* **34**, 352 (2019).
16. Stoll S., Schweiger A., *Journal of Magnetic Resonance* **178**, 42 (2006).
17. Li Y., Ooi C. P., Philip Hong Ning C., Aik Khor K., *International Journal of Applied Ceramic Technology* **6**, 501 (2009).
18. Yasukawa A., Gotoh K., Tanaka H., Kandori K., *Colloids and Surfaces A: Physicochemical and Engineering Aspects* **393**, 53 (2012).
19. Qureshi N., Malkin B., Riberolles S., Ritter C., Ouladdiaf B., Balakrishnan G., Hatnean M. C., Petrenko O., *Physical Review B* **105**, 014425 (2022).
20. Roessler M. M., Salvadori E., *Chemical Society Reviews* **47**, 2534 (2018).
21. Cugunov L., Mednis A., Kliava J., *Journal of Physics: Condensed Matter* **3**, 8017 (1991).

22. Singh V., Devi C. B. A., Rao B., Rao A., Singh N., Mistry B. M., *Optik* **226**, 165932 (2021).
23. Murali A., Chakradhar R. S., Rao J. L., *Physica B: Condensed Matter* **364**, 142 (2005).
24. Szyczewski A., Lis S., Kruczyński Z., But S., *Journal of Alloys and Compounds* **341**, 307 (2002).
25. Goldberg M., Gafurov M., Makshakova O., Smirnov V., Komlev V., Barinov S., Kudryavtsev E., Sergeeva N., Achmedova S., Mamin G., Murzakhanov F., Orlinskii S., *The Journal of Physical Chemistry B* **123**, 9143 (2019).
26. Sadovnikova M. A., Murzakhanov F. F., Fadeeva I. V., Forysenkova A. A., Deyneko D. V., Mamin G. V., Gafurov M. R., *Ceramics* **5**, 1154 (2022).
27. McGeehin P., Henderson B., *Journal of Physics C: Solid State Physics* **7**, 3988 (1974).
28. Orbach R., *Proceedings of the Royal Society of London. Series A. Mathematical and Physical Sciences* **264**, 458 (1961).
29. Aime S., Botta M., Terreno E., *Advances in Inorganic Chemistry* **57**, 173 (2005).
30. Gafurov M., Biktagirov T., Mamin G., Orlinskii S., *Applied Magnetic Resonance* **45**, 1189 (2014).
31. Shurtakova D., Mamin G., Gafurov M., *Magnetic Resonance in Solids* **25**, 23201 (2023).
32. Murzakhanov F. F., Grishin P. O., Goldberg M. A., Yavkin B. V., Mamin G. V., Orlinskii S. B., Fedotov A. Y., Petrakova N. V., Antuzevics A., Gafurov M. R., Komlev V. S., *Applied Sciences* **11**, 7727 (2021).
33. Gafurov M., Biktagirov T., Mamin G., Klimashina E., Putlayev V., Kuznetsova L., Orlinskii S., *Physical Chemistry Chemical Physics* **17**, 20331 (2015).
34. Gafurov M. R., Biktagirov T., Mamin G. V., Shurtakova D. V., Klimashina E. S., Putlyaev V., Orlinskii S. B., *Physics of the Solid State* **58**, 469 (2016).